

Solid confirmation of the broad DIB around 864.8 nm using stacked Gaia-RVS spectra

H. Zhao, M. Schultheis, T. Zwitter, C. A. L. Bailer-Jones, P. Panuzzo, P. Sartoretti, G. M. Seabroke, A. Recio-Blanco, P. de Laverny, G. Kordopatis, et al.

▶ **To cite this version:**

H. Zhao, M. Schultheis, T. Zwitter, C. A. L. Bailer-Jones, P. Panuzzo, et al.. Solid confirmation of the broad DIB around 864.8 nm using stacked Gaia-RVS spectra. Astronomy and Astrophysics - A&A, 2022, 666, 10.1051/0004-6361/202244343 . insu-03828814

HAL Id: insu-03828814
https://insu.hal.science/insu-03828814

Submitted on 25 Oct 2022

HAL is a multi-disciplinary open access archive for the deposit and dissemination of scientific research documents, whether they are published or not. The documents may come from teaching and research institutions in France or abroad, or from public or private research centers.

L'archive ouverte pluridisciplinaire **HAL**, est destinée au dépôt et à la diffusion de documents scientifiques de niveau recherche, publiés ou non, émanant des établissements d'enseignement et de recherche français ou étrangers, des laboratoires publics ou privés.



Distributed under a Creative Commons Attribution 4.0 International License

A&A 666, L12 (2022)
https://doi.org/10.1051/0004-6361/202244343
© H. Zhao et al. 2022

Astronomy & Astrophysics

LETTER TO THE EDITOR

Solid confirmation of the broad DIB around 864.8 nm using stacked *Gaia*–RVS spectra⋆

H. Zhao (赵赫)[1,2], M. Schultheis[1], T. Zwitter[3], C. A. L. Bailer-Jones[4], P. Panuzzo[5], P. Sartoretti[5], G. M. Seabroke[6], A. Recio-Blanco[1], P. de Laverny[1], G. Kordopatis[1], O. L. Creevey[1], T. E. Dharmawardena[4], Y. Frémat[7], R. Sordo[8], R. Drimmel[9], D. J. Marshall[10], P. A. Palicio[1], G. Contursi[1], M. A. Álvarez[11], S. Baker[6], K. Benson[6], M. Cropper[6], C. Dolding[6], H. E. Huckle[6], M. Smith[6], O. Marchal[12], C. Ordenovic[1], F. Pailler[13], and I. Slezak[1]

[1] University Côte d'Azur, Observatory of the Côte d'Azur, CNRS, Lagrange Laboratory, Observatory Bd, CS 34229, 06304 Nice Cedex 4, France
e-mail: he.zhao@oca.eu; mathias.schultheis@oca.eu
[2] Purple Mountain Observatory, Chinese Academy of Sciences, Nanjing 210023, PR China
[3] Faculty of Mathematics and Physics, University of Ljubljana, Jadranska 19, 1000 Ljubljana, Slovenia
[4] Max Planck Institute for Astronomy, Königstuhl 17, 69117 Heidelberg, Germany
[5] GEPI, Observatoire de Paris, Université PSL, CNRS, 5 Place Jules Janssen, 92190 Meudon, France
[6] Mullard Space Science laboratory, University College London, Holmbury St Mary, Dorking, Surrey RH5 6NT, UK
[7] Royal Observatory of Belgium, 3 Avenue Circulaire, 1180 Brussels, Belgium
[8] INAF – Osservatorio Astronomico di Padova, Vicolo Osservatorio 5, 35122 Padova, Italy
[9] INAF – Osservatorio Astrofisico di Torino, Via Osservatorio 20, 10025 Pino Torinese, Italy
[10] IRAP, Université de Toulouse, CNRS, UPS, CNES, 9 Av. Colonel Roche, BP 44346, 31028 Toulouse Cedex 4, France
[11] CIGUS CITIC – Department of Computer Science and Information Technologies, University of A Coruña, Campus de Elviña s/n, A Coruña 15071, Spain
[12] Université de Strasbourg, CNRS, Observatoire astronomique de Strasbourg, UMR 7550, 11 rue de l'Université, 67000 Strasbourg, France
[13] CNES Centre Spatial de Toulouse, 18 Avenue Edouard Belin, 31401 Toulouse Cedex 9, France

Received 24 June 2022 / Accepted 30 September 2022

ABSTRACT

Context. Studies of the correlation between different diffuse interstellar bands (DIBs) are important for exploring their origins. However, the *Gaia*–RVS spectral window between 846 and 870 nm contains few DIBs, the strong DIB at 862 nm being the only convincingly confirmed one.
Aims. Here we attempt to confirm the existence of a broad DIB around 864.8 nm and estimate its characteristics using the stacked *Gaia*–RVS spectra of a large number of stars. We study the correlations between the two DIBs at 862 nm (λ862) and 864.8 nm (λ864.8), as well as the interstellar extinction.
Methods. We obtained spectra of the interstellar medium (ISM) absorption by subtracting the stellar components using templates constructed from real spectra at high Galactic latitudes with low extinctions. We then stacked the ISM spectra in Galactic coordinates (ℓ, b) – pixelized by the HEALPix scheme – to measure the DIBs. The stacked spectrum is modeled by the profiles of the two DIBs, Gaussian for λ862 and Lorentzian for λ864.8, and a linear continuum. We report the fitted central depth (CD), central wavelength, equivalent width (EW), and their uncertainties for the two DIBs.
Results. We obtain 8458 stacked spectra in total, of which 1103 (13%) have reliable fitting results after applying numerous conservative filters. This work is the first of its kind to fit and measure λ862 and λ864.8 simultaneously in cool-star spectra. Based on these measurements, we find that the EWs and CDs of λ862 and λ864.8 are well correlated with each other, with Pearson coefficients (r_p) of 0.78 and 0.87, respectively. The full width at half maximum (FWHM) of λ864.8 is estimated as 1.62 ± 0.33 nm which compares to 0.55 ± 0.06 nm for λ862. We also measure the vacuum rest-frame wavelength of λ864.8 to be $\lambda_0 = 864.53 \pm 0.14$ nm, smaller than previous estimates.
Conclusions. We find solid confirmation of the existence of the DIB around 864.8 nm based on an exploration of its correlation with λ862 and estimation of its FWHM. The DIB λ864.8 is very broad and shallow. That at λ862 correlates better with $E(BP - RP)$ than λ864.8. The profiles of the two DIBs could strongly overlap with each other, which contributes to the skew of the λ862 profile.

Key words. ISM: lines and bands

⋆ The fitting results for all stacked spectra are only available at the CDS via anonymous ftp to cdsarc.u-strasbg.fr (130.79.128.5) or via http://cdsarc.u-strasbg.fr/viz-bin/cat/J/A+A/666/L12

Open Access article, published by EDP Sciences, under the terms of the Creative Commons Attribution License (https://creativecommons.org/licenses/by/4.0), which permits unrestricted use, distribution, and reproduction in any medium, provided the original work is properly cited.
This article is published in open access under the Subscribe-to-Open model. Subscribe to A&A to support open access publication.

1. Introduction

Diffuse interstellar bands (DIBs) are a set of absorption features with profiles that are much broader than those of the interstellar atomic lines (e.g., Na I lines). To date, over 600 DIBs have been identified at optical and near-infrared wavelengths (0.4–2.4 μm; Galazutdinov et al. 2017, Fan et al. 2019). However, our knowledge about their origins is still very limited. So far, only C_{60}^{+} has been confirmed as the carrier for five DIBs between 930 and 965 nm (see Linnartz et al. 2020 for a review). Gas-phase carbon-bearing molecules are thought to be the most probable DIB carriers (e.g., Snow et al. 2014).

Despite the unknown nature of DIBs, absorption intensity maps have been built for several such features detected in large spectroscopic surveys (e.g., Kos et al. 2014; Zasowski et al. 2015; Baron et al. 2015b; Lan et al. 2015; Puspitarini et al. 2015) in order to explore the interstellar medium (ISM) and Galactic structure. Among them, the latest map was built for the DIB at 862 nm (DIB λ862) using data from the *Gaia* Radial Velocity Spectrometer (RVS; Seabroke et al., in prep.) in Data Release 3, which has the largest sky coverage to date (see Gaia Collaboration 2022d for more details). Their wavelengths and line widths are expressed in nanometers following the unit used in the *Gaia* analysis, while their strength is still expressed in Ångströms due to their small line depth ($\lesssim$6%). The mentioned wavelengths in this paper are in the vacuum.

Studies of the correlation between different DIBs are important for identifying their origins (e.g., Friedman et al. 2011; Elyajouri et al. 2017). However, such studies are difficult for λ862 because the RVS spectral window (846–870 nm) has very few DIBs. In the review of possible DIBs in this region by Munari et al. (2008), the most promising one was thought to be located around 864.8 nm (λ864.8) with a very shallow profile. λ864.8 was first reported by Sanner & Snell (1978) following positive support from Herbig & Leka (1991), Jenniskens & Desert (1994), and Wallerstein et al. (2007). This DIB was clearly seen in spectra of early-type stars, but its analysis is complex because of the wing of the hydrogen Paschen 13 line and other stellar components. On the other hand, this band was not reported by Fan et al. (2019). Krełowski et al. (2019) argued that this feature was of stellar origin (He I lines) as it did not correlate with dust extinction. However, Baron et al. (2015a) confirmed weak correlations between dust extinction and many DIBs, which weakens this argument. Furthermore, a position correlation with dust extinction could be seen around 865 nm in Fig. 2 in Baron et al. (2015a), strengthening the DIB hypothesis for this feature.

In this work, we use the unique set of *Gaia*–RVS spectra of cool stars observed over the whole sky which has just been published as part of the third *Gaia* data release (DR3; Gaia Collaboration 2016, 2022e). We aim to confirm λ864.8 as a broad DIB rather than a stellar component by the use of stacked *Gaia*–RVS spectra to detect it and then analysis of its correlations with dust extinction and DIB λ862.

2. Data

The *Gaia*–RVS spectra have a wavelength coverage of [846−870] nm and a medium resolution of $R \sim 11\,500$ (Cropper et al. 2018). The stellar parameters and chemical abundances, including effective temperature ($T_{\rm eff}$), surface gravity ($\log g$), mean metallicity ([M/H]), and individual abundances of up to 13 chemical species, are derived by the General Stellar Parametrizer from spectroscopy (*GSP-Spec*) module of the Astrophysical parameters inference system (Apsis, Gaia Collaboration 2022b,c). We refer to Gaia Collaboration (2022c) for detailed descriptions of the parametrization and a validation of the measurement of λ862 in individual RVS spectra.

About one million *Gaia*–RVS spectra have been published in *Gaia* DR3. We use a sample of 648 944 spectra that meet the following criteria (given as an ADQL query example in Appendix A):

1. Stellar parameters ($T_{\rm eff}$, $\log g$, [M/H]) and radial velocity ($V_{\rm rad}$) are not NaN values.
2. $3500\,{\rm K} \leqslant T_{\rm eff} \leqslant 7500\,{\rm K}$ and $\log g < 6$ dex.
3. Stellar distances derived from parallax measurements ($1/\varpi$) are within 6 kpc.
4. The signal-to-noise ratios (S/N) of the observed spectra are greater than 20.
5. The uncertainty of $V_{\rm rad}$ is smaller than $5\,{\rm km\,s^{-1}}$.

This work processes stars with $T_{\rm eff} \leqslant 7500\,{\rm K}$, defined as "cool stars". The whole sample is separated into two parts: 75 941 "reference spectra" at high latitudes ($|b| \geqslant 30°$) and with low extinctions ($E(BP-RP) < 0.02$ mag) are used to construct the stellar templates for the cool stars; the other 573 003 are the "target spectra" in which we attempt to fit and measure the two DIBs. The reddening $E(BP-RP)$ used in this work was derived by the *GSP-Phot* module using their BP/RP spectra (Gaia Collaboration 2022a). Our sample uses about one-tenth of the total RVS spectra processed by *GSP-Spec* (Gaia Collaboration 2022c). Kos et al. (2013) and Lan et al. (2015) made use of a similar number of spectra in their studies. Baron et al. (2015a,b) used over 1.5 million extragalactic spectra. The large samples enable us to measure very weak DIBs by binning the spectra in large numbers.

3. Method

This work is the first of its kind to fit and measure λ862 and λ864.8 simultaneously in cool-star spectra. To do so, first we derive the ISM spectrum for each target by subtracting their stellar components using the reference spectra. We then stack the ISM spectra of the targets according to their Galactic coordinates (ℓ, b), per HEALPix. Finally we fit and measure the two DIBs, λ862 and λ864.8, in the stacked spectra.

The first step follows the main principles of Kos et al. (2013). For a given target, we find a set of reference spectra with similar parameters to the *GSP-spec* values of the target that have $T_{\rm eff} \pm 20\%$, $\log g \pm 0.6$ dex, and [M/H] $\pm$ 0.4 dex. These ranges are arbitrary, but chosen to be larger than the parameter uncertainties (Kos et al. 2013). The constraints on the stellar parameters are not necessary but they can speed up the procedure. The similarity between the target spectrum and each reference spectrum is then calculated as the average absolute difference of their flux at all pixels, except a masked region of 860–868 nm where the two DIBs are located. When measuring the difference, the central regions of the Ca II triplet are down-weighted to 30% because Ca II lines dominate the whole *Gaia*–RVS spectra of cool stars whereas the similarity between Fe I lines (close to DIBs) is more important than between the Ca II lines for constructing the templates (see examples in Contursi et al. 2021). In practice, the two Ca II regions of concern are defined as 849.43–851.03 nm and 853.73–855.73 nm and are down-weighted. The Ca II line near 866.5 nm is within the masked DIB region. Reference spectra with average differences of greater than the inverse of the square of the target S/N are discarded. For the rest, up to 500 (and at least 10) best-matching reference spectra are aver-

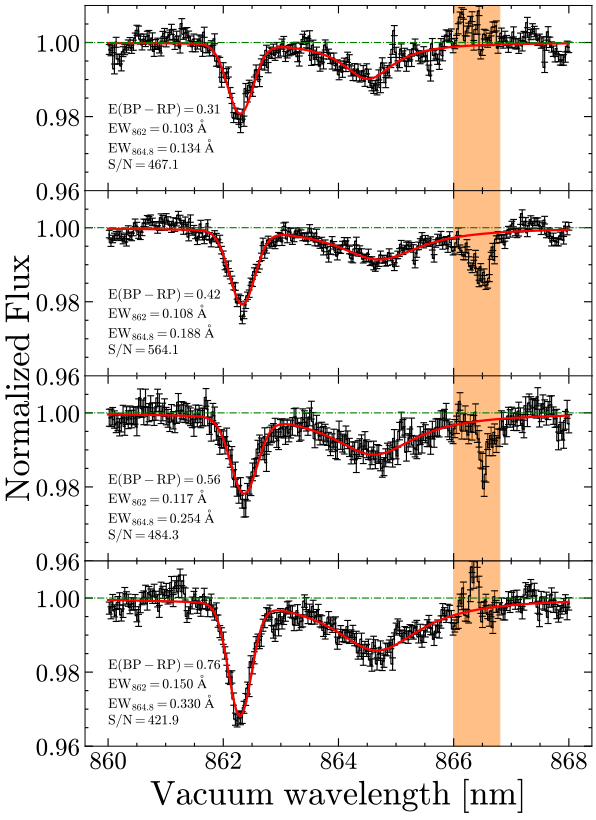


Fig. 1. Four examples of the fits to DIBs λ862 and λ864.8 in stacked *Gaia*–RVS spectra. The black lines are the ISM spectra normalized by the fitted linear continuum. The error bars indicate the flux uncertainties at each pixel. The red lines are the fitted curves that are normalized by the continuum as well. Orange marks the Ca II line residuals. The median $E(BP - RP)$ and EWs of the two DIBs in each HEALPix are also indicated.

aged and weighted by their S/N in order to build a stellar template. The target spectrum divided by the template then gives the ISM spectrum for this target. An illustration of this method can be found in Fig. 2 in Kos et al. (2013). Examples of RVS spectra and successful measurements of the DIB λ862 in individual RVS spectrum can be found in Gaia Collaboration (2022c).

In the second step, the ISM spectra are stacked according to their Galactic coordinates (ℓ, b) to get a sufficiently high S/N for a reliable measurement of λ864.8. The pixelation of the sky is done by the HEALPix[1] (Górski et al. 2005) scheme. We choose level 5 ($N_{\rm side}$ = 32), corresponding to 12 288 pixels and a spatial resolution about 1.8°. We note that 8458 HEALPix pixels (69% of the total) contain at least ten targets that have ISM spectra ($N_{\rm tar}$ > 10). In each of these pixels, we stack all of the ISM spectra (54 on average with a maximum of 362) to generate one stacked spectrum. We stack the ISM spectra in each pixel by taking the median value of the fluxes in order to reduce the influence of outliers. The flux uncertainty of the stacked spectrum is the mean of the individual flux uncertainties divided by $\sqrt{N_{\rm tar}}$, which is the standard error in the mean. The S/N of the stacked spectra is calculated between 860.2 and 861.2 nm as mean(flux)/std(flux). We have 8458 stacked spectra in total, one for each HEALPix pixel.

In the third and final step, a Markov chain Monte Carlo (MCMC) procedure (Foreman-Mackey et al. 2013) is used to fit each stacked spectrum between 860 and 868 nm (the DIB region) with a Gaussian function for the profile of λ862, a Lorentzian function (better than Gaussian when considering the goodness of fit to the line wings) for the profile of λ864.8, and a linear function for the continuum placement, masking 866–866.8 nm for the Ca II line residuals. The best estimates and statistical uncertainties are taken in terms of the 50th, 16th, and 84th percentiles of the posterior distribution. We note that the Ca II region slightly changes after the shifting to the heliocentric frame, considering that the radial velocities of most stars lie mainly within ±50 km s^{-1}, corresponding to $|\Delta\lambda| \simeq 0.14$ nm at 866.5 nm. Furthermore, the wings of the Ca II lines are better modeled than their central parts (Gaia Collaboration 2022b,c). Thus, our masked region can properly prevent contamination by the Ca II residuals and consequently the λ864.8 profile can be fitted well. Figure 1 shows four fitting examples sorted by the median $E(BP - RP)$ in each HEALPix pixel. The fitting results for all stacked spectra are available online.

Besides the fitted central depth (CD) and central wavelength ($\lambda_{\rm C}$) of the DIB profiles, the full width at half maximum (FWHM) and equivalent width (EW) are also calculated. The EW errors are estimated by the span of the profile (3 × FWHM), the pixel resolution ($\delta\lambda$ = 0.03 nm pixel^{-1}), and the noise level of the line center ($R_{\rm C}$ = std(data-model)), as $\Delta{\rm EW} = \sqrt{6\,{\rm FWHM}\,\delta\lambda} \times R_{\rm C}$, similar to the formulas given by Vos et al. (2011) and Vollmann & Eversberg (2006).

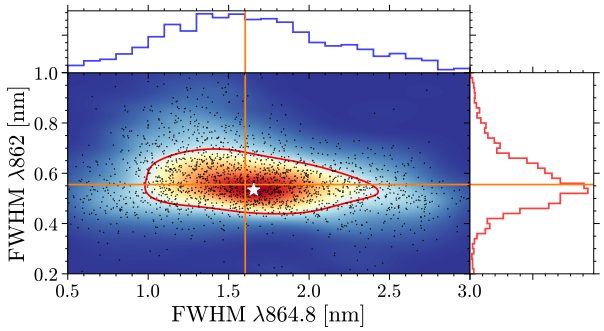


Fig. 2. Distributions of the FWHM of λ862 (red histogram) and λ864.8 (blue histogram), as well as their joint distribution (middle colored map), measured in 1962 stacked spectra after applying the general filtering. The colors represent the densities of the joint FWHM distribution, estimated by a Gaussian KDE. The white star indicates the peak density. The red line in the *central panel* indicates a contour with a probability density of 1.2, about one-third of the peak density. The orange lines indicate the median FWHM of λ862 and λ864.8, respectively.

4. Results

The aforementioned fit of the DIB was done for each of the 8458 stacked spectra (one per HEALPix pixel). To get reliable results, we only retain the stacked spectra that meet the following criteria, which leaves us with 1962 spectra:

- S/N of the stacked ISM spectrum is greater than 100.
- $\mathrm{CD}_{862} > 3R_{\rm C}$ and $\mathrm{CD}_{864.8} > R_{\rm C}$.
- The FWHM of λ862 and λ864.8 are greater than 0.2 nm and 0.5 nm, respectively.

Figure 2 shows the distributions of the FWHM of λ862 and λ864.8, as well as their joint distribution, for the 1962 stacked spectra. The FWHM of λ864.8 has a much wider distribution than that of λ862, and both slightly deviate from a Gaussian. We apply a Gaussian kernel density estimation (KDE) to their

[1] https://healpix.sourceforge.io

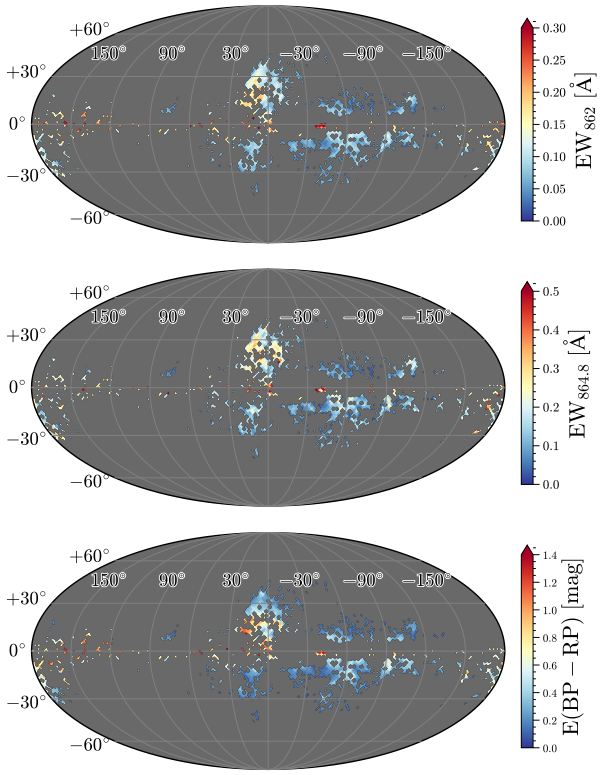


Fig. 3. Galactic distributions of the 1103 reliable measurements of the strength of λ862 (*top*), λ864.8 (*middle*), and $E(BP-RP)$ (*bottom*), in Mollweide projection, with the Galactic center in the middle and Galactic longitude increasing to the left.

joint distribution with a bandwidth of 0.2826 nm (automatically determined by the Python package *scipy*). The median FWHM is to the upper left of the peak density estimated by the KDE (white star in Fig. 2), which is caused by the fits to some very shallow profiles that result in broader λ862 and narrower λ864.8. The outliers in low-density regions are due to the noise in stacked spectra.

Therefore, we discard the points that lie in the region with a density of less than 1.2 (red line in Fig. 2), which is about one-third of the peak density. After this final filtering, our sample comprises 1103 reliable measurements of the two DIBs, about 13% of the total stacked spectra.

The two-dimensional intensity map of λ862 and λ864.8 as well as $E(BP-RP)$ are shown in Galactic coordinates in Fig. 3. Limited by our sample, the spatial distributions of EW_{862} and $\mathrm{EW}_{864.8}$ cannot be well described. However, it is clear that large EWs for both λ862 and λ864.8 concentrate in the Galactic plane. Furthermore, decreasing EW_{862} and $\mathrm{EW}_{864.8}$ with latitude (up to $b = \pm 30°$) can be found near Galactic center (GC, $|\ell| < 30°$), which are similar to each other and that of $E(BP-RP)$.

Intensity correlations between λ862, λ864.8, and $E(BP-RP)$ are shown in Fig. 4. For $E(BP-RP)$, we use $\mathrm{std}(E(BP-RP))/\sqrt{N}$ to represent its uncertainty in each HEALPix pixel. EW_{862} and $\mathrm{EW}_{864.8}$ are well correlated with each other with a Pearson coefficient of $r_\mathrm{p} = 0.78$. A systematic deviation can be seen when $\mathrm{EW}_{862} \gtrsim 0.2$ Å. The cause of this is unclear: either it has a physical origin or is due to the FWHM dispersion seen in Fig. 2. To avoid this effect, we apply simple linear fits with 2σ clipping and zero intercept for EWs and dust reddening, resulting in the following relations:

$$\begin{aligned} \mathrm{EW}_{864.8} &= 1.651(\pm0.011) \times \mathrm{EW}_{862} \\ E(BP-RP) &= 3.627(\pm0.021) \times \mathrm{EW}_{862} \\ E(BP-RP) &= 1.953(\pm0.017) \times \mathrm{EW}_{864.8} \\ \mathrm{CD}_{864.8} &= 0.368(\pm0.004) \times \mathrm{CD}_{862} + 0.002(\pm0.0001) \end{aligned} \quad . \quad (1)$$

We also apply the linear fits without any clipping. For the two DIBs, the coefficient from the no-clipping fit becomes 6% lower (1.548 ± 0.015) for their EWs and 5% lower (0.350 ± 0.006) for their CDs, compared to the 2σ-clipped results. The relative strength between DIB and dust is 13% above for λ862 ($E(BP-RP)/EW_{862} = 4.096 \pm 0.038$) and 21% above for λ864.8 ($E(BP-RP)/\mathrm{EW}_{864.8} = 2.367 \pm 0.034$), respectively, when not clipping. This is not surprising, as significant scatter about the fit can be found around $E(BP-RP) \sim 1$ mag and $\mathrm{EW}_{862} \sim 0.1$ Å. Similar scatter exists for λ864.8 as well, but this latter is more significant. This scattering could be a result of the overestimation of $E(BP-RP)$ as seen in Fig. 7 in Gaia Collaboration (2022d). We prefer the 2σ-clipped results because the scattering is not only caused by the measurement uncertainties but may indicate a spatial disconnection between their carriers and dust grains. Thus, the fitted coefficients with a strong filtering would represent their mean relative strength in the regions where these ISM materials are well mixed.

Compared to EWs, the CDs of the two DIBs are better correlated with each other with $r_\mathrm{p} = 0.87$ and no systematic deviations. The depth of λ864.8 is about 37% of that of λ862, while its EW is over 1.6 times EW_{862}. We note that EW_{862} shows good correlation with $E(BP-RP)$ with $r_\mathrm{p} = 0.85$ as expected, but their relative strength is about 20% below that derived from the DIB sample in *Gaia*-DR3 (4.507 ± 0.137, Gaia Collaboration 2022d). The reason could be that different templates – from *GSP-Spec* and from reference spectra – would introduce differences in EW measurements (see e.g., Elyajouri & Lallement 2019). It should also be noted that $E(BP-RP)/\mathrm{EW}_{862}$ fitted in this work with no clipping is closer to the result in Gaia Collaboration (2022d, 9% difference) where the authors did not make any filtering either. Also, λ864.8 does not correlate as well as λ862 with $E(BP-RP)$, showing a much smaller $r_\mathrm{p} = 0.64$ and a larger dispersion.

In a similar manner to Munari et al. (2008) and Zhao et al. (2021), in order to estimate the rest-frame wavelength (λ_0) of λ864.8, we assume that the median radial velocity in the Local Standard of Rest of the DIB carrier is zero toward the GC. There are 43 cases with $|\ell| \leqslant 10°$, $|b| \leqslant 10°$, and small uncertainties in λ_C (<0.1 nm for λ862 and <0.15 nm for λ864.8). For λ862, we derive a λ_0 of 862.319 ± 0.018 nm, which is highly consistent with the result of 862.323 ± 0.0019 nm in Gaia Collaboration (2022d). For λ864.8, we derive $\lambda_0 = 864.53 \pm 0.14$ nm in the vacuum, corresponding to 864.29 nm for air wavelength. This result is smaller than the commonly suggested air wavelength measured in the spectra of early-type stars, such as 865.0 nm (Sanner & Snell 1978), 864.9 nm (Herbig & Leka 1991), and 864.83 nm (Jenniskens & Desert 1994).

5. Discussion

Until now, the FWHM of the λ864.8 feature has not been well determined. Sanner & Snell (1978) noted that this DIB profile extends from 863 to 866 nm and its strength did not correlate with spectral type, but they did not measure its FWHM. We found two measurements of FWHM λ864.8 in the literature that are dramatically different from each other: 1.4 nm

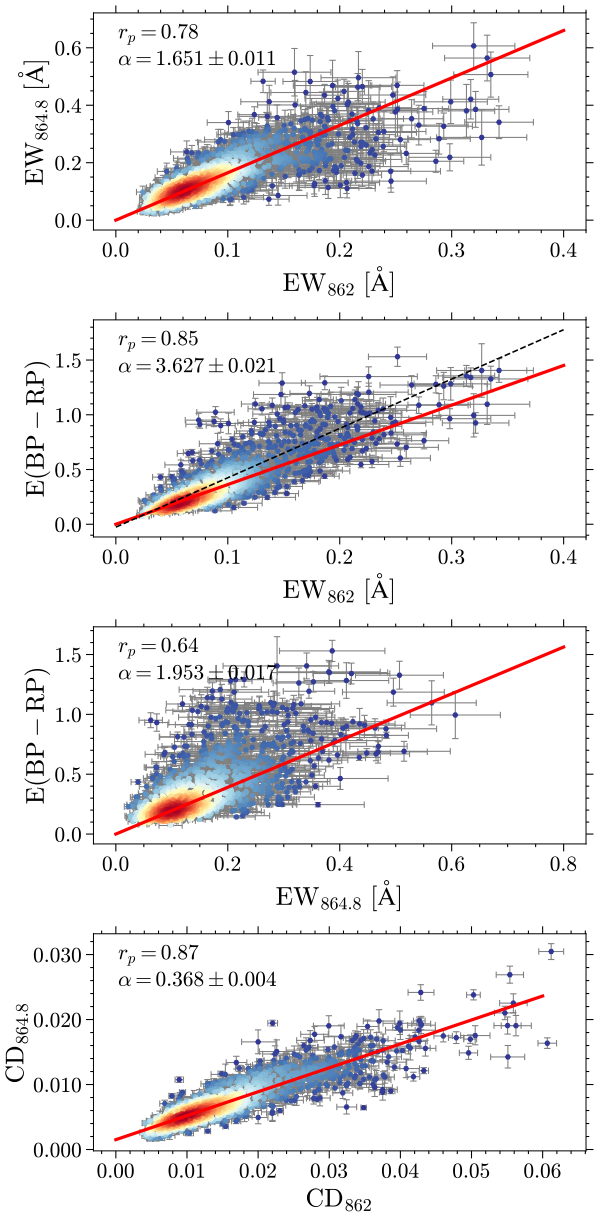


Fig. 4. Intensity correlations between λ862, λ864.8, and $E(BP - RP)$. Different correlations are shown in each panel with the Pearson coefficient (r_p) and the slope of a 2σ-clipped linear fit (α) with zero intercept shown in red. Data points with error bars are colored by their number density estimated by a Gaussian KDE. The black dashed line shown in the *second panel* from the top is the linear relation derived in Gaia Collaboration (2022d).

by Herbig & Leka (1991) and 0.42 nm by Jenniskens & Desert (1994). The difficulty is that this band is shallow and superposed across several blended stellar lines, such as the He I line at 864.83 nm in early B-type supergiants (Herbig & Leka 1991). This may be the reason why a stellar origin has been claimed in the literature (Krełowski et al. 2019). In this work, we made use of the spectra of cool stars, and subtracted the stellar lines (mainly Fe I and Ca II) using reference spectra. This makes our measurements more accurate than those previous works based on hot-star spectra. We find λ864.8 to be a very broad and shallow DIB with a FWHM of 1.62 ± 0.33 nm, which is not significantly less than the strongest DIB at 442.8 nm (e.g., 1.7 nm; Galazutdinov et al. 2020). This provides strong evidence for the DIB interpretation of this line because no known stellar components or Doppler broadening (a velocity dispersion over 600 km s^{-1}) can explain such a large width. On the other hand, the derived FWHM of λ862 in this work is 0.55 ± 0.06 nm, which is slightly larger than previously reported values such as 0.43 nm (Herbig & Leka 1991), 0.47 nm (Maíz Apellániz 2015), and 0.37 nm (Fan et al. 2019). The increase in FWHM could be explained by a Doppler broadening caused by our stacking strategy, with a velocity dispersion about 30–50 km s^{-1}. This value is consistent with the average magnitude of the $V_{\rm rad}$ dispersion in each pixel (about 36 km s^{-1}) which can be treated as an upper limit to the velocity dispersion of the DIB clouds, because closer objects should have a smaller radial velocity than the background stars.

Although the DIB profile could be broadened due to the superposition effect, our stacking has only a very weak influence on EW measurements, because DIBs are weak spectral features and we are therefore in a linear regime where the EW produced by multiple DIB clouds can be simply added up (Munari & Zwitter 1997). The linear correlation between EW_{862} and $EW_{864.8}$ provides good evidence for a DIB interpretation of this line, in spite of the superposition effect, because the stellar components or their residuals cannot have such a behavior with interstellar features. Another important point is that the profiles of the two DIBs could be overlapped with each other. Therefore, it is better to measure the two DIBs simultaneously; although this requires a very high S/N.

Limited by our sample and the conservative approach to filtering it, further analysis of the two DIBs – such as the kinematics of their carriers and the nature of the Lorentzian profile of λ864.8 – is not feasible. Nevertheless, it is significant to confirm a second DIB close to the strong one λ862 in such a big spectroscopic survey, which enables us to use them as tracers of the ISM environment if they have different origins, or facilitates the study of their origin if they share a common carrier (with two DIBs, their relative strength and central wavelengths could provide clues as to their carrier). Dedicated research into these two DIBs will be carried out using all available RVS spectra and the results will be published in next *Gaia* data release.

6. Conclusions

Based on the measurements in 1103 stacked *Gaia*–RVS spectra, we provide solid confirmation of the DIB around 864.8 nm through its correlation with λ862 and its clear and broad profile in the stacked spectra. λ864.8 is a very broad and shallow DIB. The FWHM of λ864.8 is estimated to be 1.62 ± 0.33 nm. Using 43 high-quality measurements toward GC ($|\ell| \leqslant 10°$, $|b| \leqslant 10°$), the rest-frame wavelength of λ864.8 is determined as λ_0 = 864.53 ± 0.14 nm in the vacuum, which is smaller than previous reported measurements. EW_{862} correlates better with $E(BP - RP)$ than $EW_{864.8}$.

Our work shows the power of using a large set of cool-star spectra to study the DIBs in the ISM. The extremely small depth of these lines ($CD_{864.8} \lesssim 3\%$) and the ability to assess their properties is a clear demonstration of the quality of *Gaia*–RVS spectra as published in *Gaia* DR3.

Acknowledgements. This work has made use of data from the European Space Agency (ESA) mission *Gaia* (https://www.cosmos.esa.int/gaia), processed by the *Gaia* Data Processing and Analysis Consortium (DPAC, https://www.cosmos.esa.int/web/gaia/dpac/consortium). Funding for the DPAC has been provided by national institutions, in particular the

institutions participating in the *Gaia* Multilateral Agreement. This work was supported in part by: the German Aerospace Agency (DLR) grant 50 QG 2102; SFB 881 "The Milky Way System" of the German Research Foundation (DFG).

References

Baron, D., Poznanski, D., Watson, D., et al. 2015a, MNRAS, 451, 332
Baron, D., Poznanski, D., Watson, D., Yao, Y., & Prochaska, J. X. 2015b, MNRAS, 447, 545
Contursi, G., de Laverny, P., Recio-Blanco, A., & Palicio, P. A. 2021, A&A, 654, A130
Cropper, M., Katz, D., Sartoretti, P., et al. 2018, A&A, 616, A5
Elyajouri, M., & Lallement, R. 2019, A&A, 628, A67
Elyajouri, M., Lallement, R., Monreal-Ibero, A., Capitanio, L., & Cox, N. L. J. 2017, A&A, 600, A129
Fan, H., Hobbs, L. M., Dahlstrom, J. A., et al. 2019, ApJ, 878, 151
Foreman-Mackey, D., Hogg, D. W., Lang, D., & Goodman, J. 2013, PASP, 125, 306
Friedman, S. D., York, D. G., McCall, B. J., et al. 2011, ApJ, 727, 33
Gaia Collaboration (Prusti, T., et al.) 2016, A&A, 595, A1
Gaia Collaboration (Andrae, R., et al.) 2022a, A&A, in press https://doi.org/10.1051/0004-6361/202243462
Gaia Collaboration (Creevey, O. L., et al.) 2022b, A&A, in press https://doi.org/10.1051/0004-6361/202243688
Gaia Collaboration (Recio-Blanco, A., et al.) 2022c, A&A, in press https://doi.org/10.1051/0004-6361/202243750
Gaia Collaboration (Schultheis, M., et al.) 2022d, A&A, in press https://doi.org/10.1051/0004-6361/202243283
Gaia Collaboration (Vallenari, A., et al.) 2022e, A&A, in press https://doi.org/10.1051/0004-6361/202243940
Galazutdinov, G. A., Lee, J.-J., Han, I., et al. 2017, MNRAS, 467, 3099
Galazutdinov, G., Bondar, A., Lee, B.-C., et al. 2020, AJ, 159, 113
Górski, K. M., Hivon, E., Banday, A. J., et al. 2005, ApJ, 622, 759
Herbig, G. H., & Leka, K. D. 1991, ApJ, 382, 193
Jenniskens, P., & Desert, F. X. 1994, A&AS, 106, 39
Kos, J., Zwitter, T., Grebel, E. K., et al. 2013, ApJ, 778, 86
Kos, J., Zwitter, T., Wyse, R., et al. 2014, Science, 345, 791
Krełowski, J., Galazutdinov, G., Godunova, V., & Bondar, A. 2019, Acta Astron., 69, 159
Lan, T.-W., Ménard, B., & Zhu, G. 2015, MNRAS, 452, 3629
Linnartz, H., Cami, J., Cordiner, M., et al. 2020, J. Mol. Spectrosc., 367, 111243
Maíz Apellániz, J. 2015, Mem Soc. Astron. It., 86, 553
Munari, U., & Zwitter, T. 1997, A&A, 318, 269
Munari, U., Tomasella, L., Fiorucci, M., et al. 2008, A&A, 488, 969
Puspitarini, L., Lallement, R., Babusiaux, C., et al. 2015, A&A, 573, A35
Sanner, F., Snell, R., & vanden Bout, P., 1978, ApJ, 226, 460
Snow, T. P. 2014, in The Diffuse Interstellar Bands, eds. J. Cami, & N. L. J. Cox, 297, 3
Vollmann, K., & Eversberg, T. 2006, Astron. Nachr., 327, 862
Vos, D. A. I., Cox, N. L. J., Kaper, L., Spaans, M., & Ehrenfreund, P. 2011, A&A, 533, A129
Wallerstein, G., Sandstrom, K., & Gredel, R. 2007, PASP, 119, 1268
Zasowski, G., Ménard, B., Bizyaev, D., et al. 2015, ApJ, 798, 35
Zhao, H., Schultheis, M., Rojas-Arriagada, A., et al. 2021, A&A, 654, A116

Appendix A: ADQL queries

```
SELECT *
FROM gaiadr3.astrophysical_parameters AS gaia
INNER JOIN gaiadr3.gaia_source AS xmatch
ON gaia.source_id = xmatch.source_id
WHERE (xmatch.has_rvs='T' AND gaia.teff_gspspec > 3500 AND gaia.teff_gspspec < 7500
AND gaia.logg_gspspec < 6 AND xmatch.parallax > 0.0 AND 1/xmatch.parallax < 6  AND
xmatch.radial_velocity_error < 5.0 AND  xmatch.rv_expected_sig_to_noise > 20.0 AND
gaia.mh_gspspec is NOT NULL)
```